AMERICAN SOCIETY FOR MICROBIOLOGY | Journal of Virology®

PATHOGENESIS AND IMMUNITY

Type I Interferon Orchestrates Demand-Adapted Monopoiesis during Influenza A Virus Infection via STAT1-Mediated Upregulation of Macrophage Colony-Stimulating Factor Receptor Expression

Sue-Jane Lin,[a] Kai-Min Lin,[a] Shi-Yo Jill Chen,[a] Chia-Chi Ku,[b] Chen-Wei Huang,[c] Chi-Hsiang Huang,[d] Michael Gale, Jr.,[e] Ching-Hwa Tsai[a]

[a]Graduate Institute of Microbiology, College of Medicine, National Taiwan University, Taipei, Taiwan
[b]Institute of Immunology, College of Medicine, National Taiwan University, Taipei, Taiwan
[c]Department of Family Medicine, National Taiwan University Hospital, College of Medicine, National Taiwan University, Taipei, Taiwan
[d]Department of Internal Medicine, Linkou Chang Gung Memorial Hospital, Tao-Yuan, Taiwan
[e]Center for Innate Immunity and Immune Disease, Department of Immunology, University of Washington, Seattle, Washington, USA

ABSTRACT Whether and how a local virus infection affects the hematopoietic system in the bone marrow is largely unknown, unlike with systemic infection. In this study, we showed that influenza A virus (IAV) infection leads to demand-adapted monopoiesis in the bone marrow. The beta interferon (IFN-β) promoter stimulator 1 (IPS-1)–type I IFN–IFN-α receptor 1 (IFNAR1) axis-mediated signaling was found to induce the emergency expansion of the granulocyte-monocyte progenitor (GMP) population and upregulate the expression of the macrophage colony-stimulating factor receptor (M-CSFR) on bipotent GMPs and monocyte progenitors via the signal transducer and activator of transcription 1 (STAT1), leading to a scaled-back proportion of granulocyte progenitors. To further address the influence of demand-adapted monopoiesis on IAV-induced secondary bacterial infection, IAV-infected wild-type (WT) and *Stat1*$^{-/-}$ mice were challenged with *Streptococcus pneumoniae*. Compared with WT mice, *Stat1*$^{-/-}$ mice did not demonstrate demand-adapted monopoiesis, had more infiltrating granulocytes, and were able to effectively eliminate the bacterial infection.

IMPORTANCE Our findings show that influenza A virus infection induces type I interferon (IFN)-mediated emergency hematopoiesis to expand the GMP population in the bone marrow. The type I IFN-STAT1 axis was identified as being involved in mediating the viral-infection-driven demand-adapted monopoiesis by upregulating M-CSFR expression in the GMP population. As secondary bacterial infections often manifest during a viral infection and can lead to severe or even fatal clinical complications, we further assessed the impact of the observed monopoiesis on bacterial clearance. Our results suggest that the resulting decrease in the proportion of granulocytes may play a role in diminishing the IAV-infected host's ability to effectively clear secondary bacterial infection. Our findings not only provide a more complete picture of the modulatory functions of type I IFN but also highlight the need for a more comprehensive understanding of potential changes in hematopoiesis during local infections to better inform clinical interventions.

KEYWORDS influenza A virus, type I IFNs, monopoiesis, *Streptococcus pneumoniae*

Microbial infection stimulates a hematopoietic shift in the bone marrow, from a steady state to an emergency state, to combat pathogens, especially in a systemic infection (1, 2). Several signs are observed in this hematopoietic alteration, including the presence of immature blood cells in the peripheral blood, leukocytosis, and neutrophilia. In

Editor Bryan R. G. Williams, Hudson Institute of Medical Research

Address correspondence to Ching-Hwa Tsai, chtsai@ntu.edu.tw.

The authors declare no conflict of interest.

Received 18 January 2023
Accepted 14 March 2023
Published 6 April 2023

local influenza A virus (IAV) infection, monocyte-derived resident alveolar macrophages are depleted by 70 to 90% within 1 week postinfection (3). Recruited dendritic cells are also depleted by 50% 4 to 7 days postinfection (4, 5). Simultaneously, bone marrow-derived Ly6C$^+$ monocytes are predominantly recruited by C-C chemokine receptor type 2 (CCR2)-dependent chemotaxis and reach a peak 7 to 10 days post-IAV infection (6–8). Over 44% of recruited Ly6C$^+$ monocytes further differentiate into alveolar macrophages to replenish the consumed macrophages during recovery from IAV infection (9). There seems to be a compensatory mechanism to replenish the monocyte pool in the bone marrow, because there are no obvious hematopoietic alterations in the circulating blood.

In the bone marrow, hematopoietic stem cells (HSCs) are the origin of myeloid-, erythroid-, and lymphoid-lineage cells. In the myeloid lineage, multipotent progenitors (MPPs) derived from HSCs subsequently give rise to common myeloid progenitors (CMPs), which further differentiate into granulocyte-monocyte progenitors (GMPs), monocyte-dendritic progenitors (MDPs), and megakaryocyte-erythroid progenitors (MEPs) (10). Both GMPs and MDPs are bipotent cells, which can further differentiate into their downstream progenitors, granulocyte progenitors (GPs) or monocyte progenitors (MPs), and common monocyte progenitors (cMoPs) or common dendritic progenitors (CDPs), respectively. Notably, both GMPs and MDPs can generate functionally distinct Ly6C$^+$ classical monocytes (also known as inflammatory monocytes) in response to stimulation by different microbial components, such as lipopolysaccharide (LPS) and CpG DNA (10).

Hematopoietic stem and progenitor cells (HSPCs) can be activated to induce emergency hematopoiesis by direct and/or indirect sensing of pathogens (9). Direct sensing of HSPCs is evidenced by the expression of Toll-like receptors (TLRs) in response to their corresponding microbial stimuli (11). The indirect sensing of HSPCs is mediated by cytokines and hematopoietic growth factors, which are produced by infected or primed hematopoietic and nonhematopoietic cells (9, 12, 13). The effects of interferons (IFNs), interleukin 1β (IL-1β), IL-6, tumor necrosis factor (TNF), transforming growth factor β (TGF-β), macrophage colony-stimulating factor (M-CSF), granulocyte colony-stimulating factor (G-CSF), and GM-CSF on the regulation of HSPC proliferation and differentiation have been reported (9, 12, 13). In particular, type I IFN, induced by pattern recognition receptors (PRRs), plays a critical role in innate immune responses against viral infections by initiating an intracellular antimicrobial program in infected and neighboring cells as well as enhancing antigen presentation and the production of cytokines and chemokines (14). Type I IFN can also prime bone marrow leukocytes through blood circulation to limit viral replication in distal organs (15). Moreover, a constitutive low level of type I IFN is required for the maintenance of hematopoiesis in the steady state (16), and the administration of type I IFN can activate dormant HSCs to proliferate under sterile conditions (17).

Earlier studies also reported that type I IFN signaling promotes IAV-mediated secondary bacterial infections (18–21). In the clinical setting, many respiratory viruses, such as IAV, respiratory syncytial virus (RSV), rhinovirus, parainfluenza virus, severe acute respiratory syndrome coronavirus 2 (SARS-CoV-2), and adenovirus, are associated with bacterial superinfection (22). IAV is the most common cause of seasonal respiratory infections, and the increased morbidity and mortality associated with bacterial coinfection have been well documented in clinical and epidemiologic studies (22, 23). Secondary bacterial pneumonia usually occurs around 3 to 7 days post-IAV infection, with clinical characteristics including damage to the respiratory epithelium, an insufficient number of neutrophils, impaired phagocytic ability of macrophages, and prolonged production of type I IFN (20, 22–24). In the lungs, type I IFN upregulates the expression levels of monocyte chemoattractants (CCL-2, CCL-7, and CCL-12), resulting in the preferential infiltration of bone marrow-derived Ly6C$^+$ CCR2$^+$ monocytes (7, 25). Simultaneously, type I IFN suppresses the production of neutrophil chemoattractants (CXCL1/KC and CXCL2/MIP2) in macrophages, leading to a decrease in neutrophil influx (18).

In this study, we demonstrated that the type I IFN-STAT1 (signal transducer and activator of transcription 1) axis induces the expression of macrophage colony-stimulating

factor receptor (M-CSFR; also known as CSF-1R and CD115 [cluster of differentiation 115]) at the transcriptional and translational levels in the GMP population, leading to demand-adapted monopoiesis and scaled-back granulopoiesis upon acute IAV infection. Our findings identify a previously undiscovered role of type I IFN in demand-adapted monopoiesis, demonstrating an additional mechanism by which type I IFN may compromise the host's ability to clear secondary bacterial infections.

RESULTS

Expansion of the GMP population in the bone marrow was observed during IAV infection. Myeloid cells are the major infiltrates in the lungs, including neutrophils and monocyte-derived macrophages, after IAV infection (7, 26). In order to trace the migration of myeloid cells during IAV infection, we infected B6 mice with PR8 virus and monitored myeloid cells ($Gr1^+$ $CD11b^+$ cells) in the lung, mediastinal lymph nodes (MLNs), spleen, and bone marrow. Compared with uninfected mice, the proportions and numbers of myeloid cells were significantly increased in the lungs (5.9% ± 0.6% versus 55.7% ± 2.6%) and bone marrow (31.2% ± 2.6% versus 54.4% ± 2.7%) of infected mice (Fig. 1A to F). However, this phenomenon was not observed in the MLNs and spleens (Fig. 1A to D). Our findings suggest that IAV infection triggers demand-adapted myelopoiesis in the bone marrow.

To explore our assumption, HSPCs obtained from the bone marrow were classified and quantified in uninfected and infected mice. The gating of the different cell populations was based on the two-dimensional staining of six surface markers. First, we gated on IL-7Rα^- and Lin^- (lineage negative) to exclude differentiated cells and lymphoid progenitors (Fig. 1G, left). Second, the gated IL-7Rα^- Lin^- cells were further analyzed for their Sca-1 and c-Kit expression. IL-7Rα^- Lin^- $Sca\text{-}1^+$ $c\text{-}Kit^+$ cells were defined as the LSK subset, which is made up of HSCs and MPPs (Fig. 1G, middle). Third, c-Kit single-positive progenitor cells were gated (Fig. 1G, middle) and further analyzed for their FcγRII/III (also known as CD32/CD16) and CD34 expression for classification into three subpopulations: CMPs (IL-7Rα^- Lin^- $Sca\text{-}1^-$ $c\text{-}Kit^+$ FcγRII/III^{low} $CD34^+$), GMPs (IL-7Rα^- Lin^- $Sca\text{-}1^-$ $c\text{-}Kit^+$ FcγRII/III^{high} $CD34^+$), and MEPs (IL-7Rα^- Lin^- $Sca\text{-}1^-$ $c\text{-}Kit^+$ FcγRII/III$^-$ $CD34^-$) (Fig. 1G, right). The total numbers of LSK cells and CMPs did not significantly increase after infection (Fig. 1H). Meanwhile, a significant expansion of the GMP population and a dramatic decrease in MEPs were observed in infected mice (Fig. 1H). These results indicated that demand-adapted hematopoiesis leaned toward myelopoiesis rather than megakaryopoeisis/erythropoiesis. The GMP population is composed of three subsets: bipotent GMPs, MPs, and GPs (27). Using the myeloid differentiation marker Ly6C, the GMP population could be further divided into bipotent GMPs ($Ly6C^-$) and a mixed subset of MPs/GPs ($Ly6C^+$). As shown in Fig. 1I, in the GMP population, the proportion of bipotent GMPs was decreased while the proportion of MPs/GPs was increased after IAV infection, suggesting an increased differentiation of bipotent GMPs to MPs/GPs. Based on M-CSFR expression, MPs/GPs could be further grouped into MPs ($M\text{-}CSFR^+$) and GPs ($M\text{-}CSFR^-$). Compared with uninfected mice, in the mixed subset of MPs/GPs, the proportion of MPs increased from 10.7% ± 2.5% to 30.1% ± 2.1%, while the proportion of GPs decreased from 89.3% ± 2.6% to 69.9% ± 2.1% in infected mice (Fig. 1J), indicating an accelerated differentiation of bipotent GMPs to MPs.

According to our and others' previous studies, a marked accumulation of bone marrow-derived $Ly6C^+$ monocytes by CCR2-dependent recruitment in the lungs during IAV infection has been identified (7, 8, 25, 28). However, the relationship between the increase in GMP population observed here and the infiltrating $Ly6C^+$ $CCR2^+$ inflammatory macrophages described previously is unclear. Hence, to determine if the increased GMP population in the bone marrow serves as an origin of $Ly6C^+$ $CCR2^+$ monocytes during IAV infection, we adoptively transferred the GMP population from infected Ly5.1 mice to infected Ly5.2 mice and then analyzed the bone marrows of the recipients. As shown in Fig. 1K, 96 ± 0.7% of the sorted GMP population from infected Ly5.1 mice differentiated into $Gr1^+$ $CD11b^+$ myeloid cells, which mainly comprised $Ly6C^+$ $CCR2^+$ monocytes, in infected Ly5.2 recipient mice. Our results demonstrated the GMP

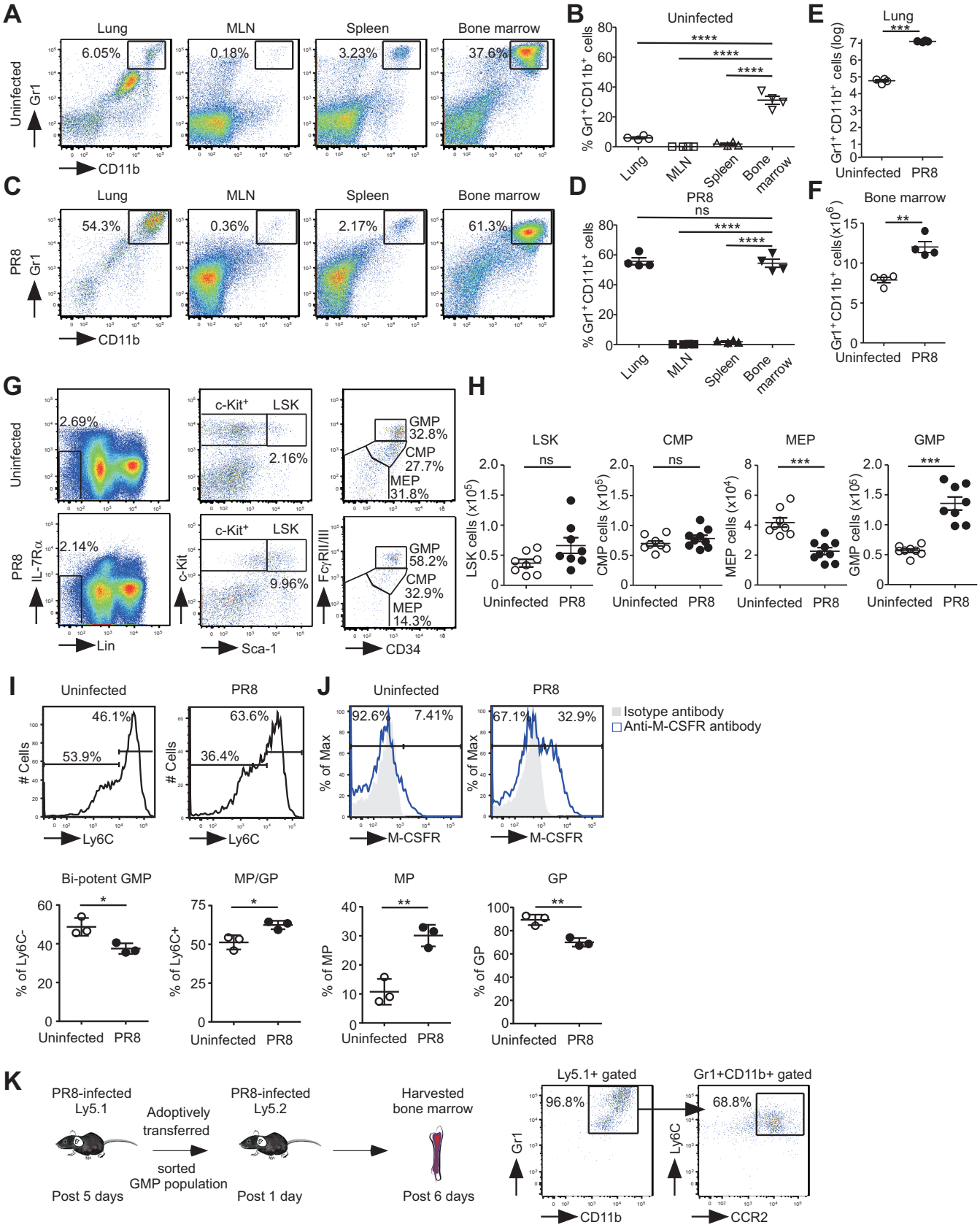

FIG 1 Demand-adapted expansion of GMPs was observed in IAV infection. (A and C) Leukocytes from the lung, MLNs, spleen, and bone marrow were harvested from the uninfected (A) and infected (C) B6 mice. Harvested cells were counted by trypan blue exclusion and assayed for the expression of Gr1

(Continued on next page)

population to be a major source of Ly6C$^+$ CCR2$^+$ monocytes following IAV infection. Thus, the expansion of the GMP population followed by the differentiation into Ly6C$^+$ CCR2$^+$ monocytes in the bone marrow after IAV infection may be an emergency homeostatic mechanism to meet the need to replenish Ly6C$^+$ CCR2$^+$ macrophages in the lungs.

Emergency expansion of the GMP population was mediated by type I IFN. Previous studies have shown that TLRs and various cytokine receptors are expressed on HSPCs (9, 12), indicating that these receptors might be involved in demand-adapted hematopoiesis during infections. To address the involvement of TLRs, RIG-like receptors (RLRs), and cytokine-triggered signaling in the observed GMP population expansion during IAV infection, we infected various mice lacking either the myeloid differentiation factor 88 (MyD88), beta interferon promoter stimulator 1 (IPS-1), or alpha interferon receptor 1 (IFNAR1) gene with IAV and then measured the expansion of the GMP population in the bone marrow. MyD88 is a key adaptor protein downstream of TLRs, except for TLR3. IPS-1 (also known as MAVS, VISA, and CARDIF) is a crucial adaptor protein downstream of RLRs (29). Recognition of viral infection by TLRs or RLRs has a cell type-specific effect on type I IFN production (30). IFNAR1 is an important subunit of the receptor for IFN-α/β; binding and activation of the receptor initiate signal transduction. As shown in Fig. 2A and B, the expansion of the GMP population was drastically reduced in infected *Ips-1*$^{-/-}$ and *Ifnar1*$^{-/-}$ mice but not in infected *Myd88*$^{-/-}$ mice, demonstrating the RLR–IFN-α/β axis to be a key player in the IAV-induced emergency expansion of the GMP population in the bone marrow.

Next, we measured the mRNA expression of IFN-β triggered by TLRs or RLRs in the infiltrating Ly6C$^+$ CCR2$^+$ monocyte-derived cells obtained from the lungs. Compared with the TLR-MyD88 axis, the RLR–IPS-1 axis played a crucial role in the induction of IFN-β in the Ly6C$^+$ CCR2$^+$ monocyte-derived cells (Fig. 2C). Furthermore, we measured the protein expression of IFN-β in the bronchoalveolar lavage fluid (BALF) of the mice. A relatively low level of IFN-β was found in infected *Ips-1*$^{-/-}$ mice, whereas a high level of IFN-β accumulated in infected *Ifnar1*$^{-/-}$ mice (Fig. 2D). In summary, knocking out IPS-1 led to impaired mRNA expression of IFN-β in the infiltrating Ly6C$^+$ CCR2$^+$ monocyte-derived cells, which was consistent with the decreased protein expression of IFN-β in the BALF of infected *Ips-1*$^{-/-}$ mice.

A previous study showed that a constitutive low-level secretion of type I IFN is critical for the homeostasis of HSCs (16). Indeed, we found that naive *Ifnar1*$^{-/-}$ mice had fewer HSCs than naive wild-type (WT) mice (data not shown). To exclude any potential influences of the lower basal HSC numbers in *Ifnar1*$^{-/-}$ mice on the GMP population proportion postinfection, IFNAR1 signaling in IAV-infected mice was blocked with anti-IFNAR1 antibody. Consistent with the results seen in *Ifnar1*$^{-/-}$ mice, IFNAR1 signaling

FIG 1 Legend (Continued)
and CD11b. Representative dot plots are shown for the indicated tissues. (B and D) Percentages of Gr1$^+$ CD11b$^+$ myeloid cells in the indicated tissues in uninfected (B) and infected (D) mice. Statistical significance was determined using Tukey's multiple-comparison test of one-way ANOVA (ns, no significant difference; ****, $P < 0.0001$). (E and F) Total numbers of Gr1$^+$ CD11b$^+$ myeloid cells in the lungs (E) and bone marrow (F) in uninfected and infected mice. Results are from a representative experiment of three repeated experiments with 4 mice per group (mean ± standard error of the mean [SEM]). Statistical significance was determined using the Student two-tailed *t* test (**, $P < 0.01$; ***, $P < 0.001$). (G and H) Bone marrow cells were isolated from the uninfected and infected B6 mice on day 7 postinfection, counted by trypan blue exclusion, and then stained with antibodies against IL-7Rα, Lin, c-Kit, Sca-1, FcγRII/III, and CD34 markers. IL-7Rα^- Lin$^-$ cells were gated and further surveyed for the expression of Sca-1 and c-Kit in gated cells. To define the populations of CMPs, GMPs, and MEPs, the expression levels of FcγRII/III and CD34 were analyzed in c-Kit$^+$ Sca-1$^-$ gated cells. (G) Representative dot plots of the Lin$^-$ population, IL-7Rα^- Lin$^-$ Sca-1$^+$ c-Kit$^+$ (LSK), c-kit$^+$ Sca-1$^-$ population, CMPs, GMPs, and MEPs are shown. (H) Total numbers of LSK cells, CMPs, MEPs, and GMPs are shown. Results are representative of three repeated experiments ($n = 8$; mean ± SEM). Statistical significance was determined using the Student two-tailed *t* test (ns, no significant difference; ***, $P < 0.001$). (I) To define the subsets of bipotent GMPs and MPs/GPs, expression of Ly6C was analyzed on gated GMP populations. Representative histograms of Ly6C expression are shown in the top panels. The percentages of Ly6C$^-$ bipotent GMPs and Ly6C$^+$ MPs/GPs are shown in the bottom panel. Results are representative of three repeated experiments, with 3 mice per group (means and SEM). Statistical significance was determined using the Student two-tailed *t* test (*, $P < 0.05$). (J) To define the subsets of MPs and GPs, expression of the M-CSFR was analyzed in gated Ly6C$^+$ MP/GP populations. Representative histograms of M-CSFR expression are shown in the top panel. The percentages of MPs and GPs are shown in the bottom panels. Results are representative of three repeated experiments, with 3 mice per group (means and SEM). Statistical significance was determined using the Student two-tailed *t* test (**, $P < 0.01$). (K) The GMP population was sorted from PR8-infected Ly5.1 mice. Sorted cells were adoptively transferred into PR8-infected Ly5.2 mice. Infected Ly5.2$^+$ recipient mice were analyzed for Ly5.1$^+$ donor bone marrow cells. The proportion of Ly6C$^+$ CCR2$^+$ monocytes in the Ly5.1$^+$ Gr1$^+$ CD11b$^+$ population was examined by flow cytometry. Results are representative of two repeated experiments, with 3 mice per group.

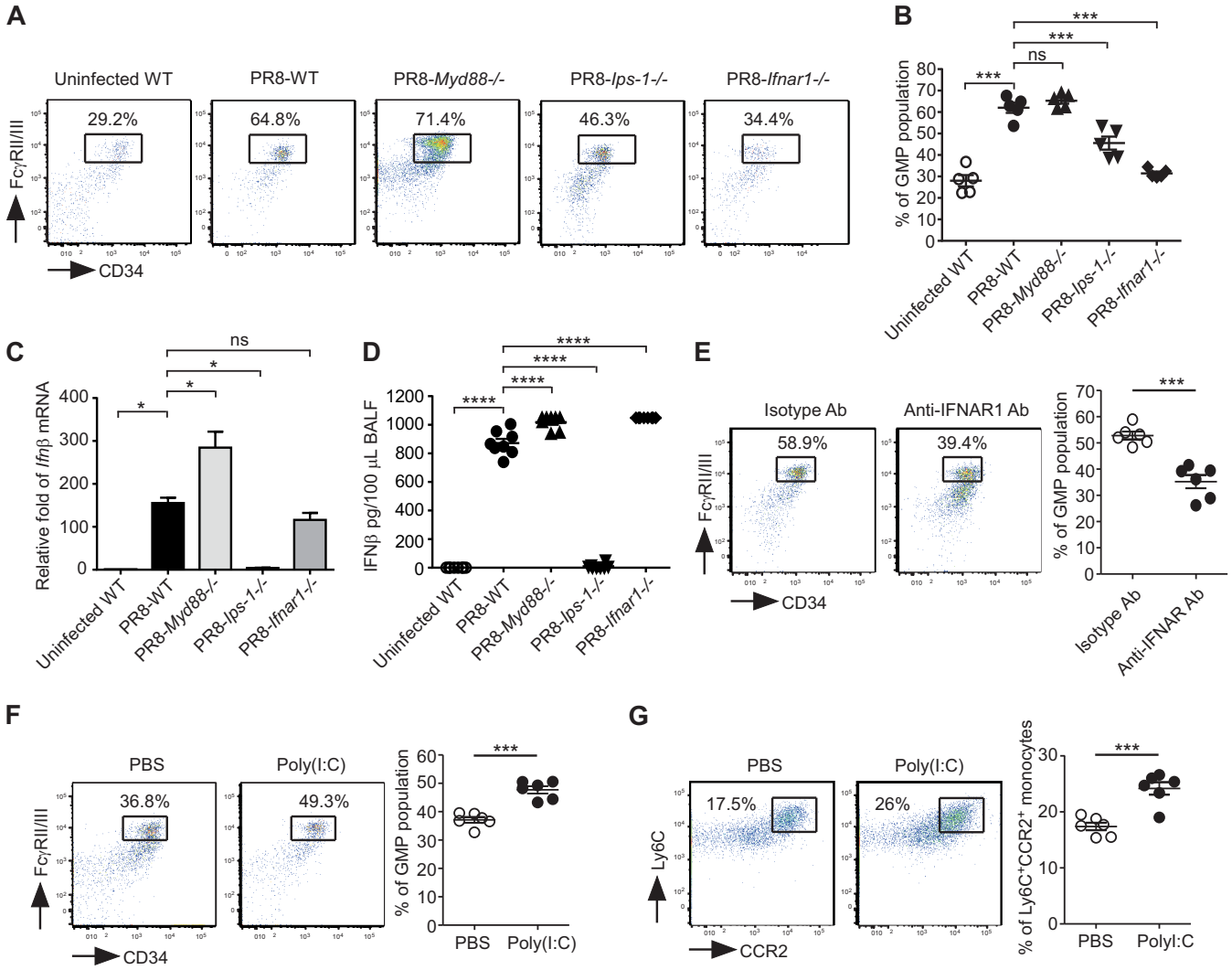

FIG 2 Type I IFN-driven emergency expansion of the GMP population. WT, *Myd88*$^{-/-}$, *Ips-1*$^{-/-}$, and *Ifnar1*$^{-/-}$ mice were infected with PR8. Bone marrow cells were harvested on day 7 postinfection. (A) Representative dot plots of the GMP population are shown for the indicated mice. (B) The percentage of the GMP population was analyzed using flow cytometry. Results are representative of three repeated experiments with 5 mice per group (means and SEM). Statistical significance was determined using Tukey's multiple-comparison test of one-way ANOVA (ns, no significant difference; ***, $P < 0.001$). (C) Expression levels of IFN-β transcripts in sorted Ly6C$^+$ CCR2$^+$ monocytes/macrophages from the lungs were measured by qRT-PCR. The relative fold expression was compared to that of the uninfected group after normalization with GAPDH expression. Statistical significance was determined using Tukey's multiple-comparison test of one-way ANOVA (ns, no significant difference; *, $P < 0.05$). (D) Expression of IFN-β in BALF was quantified by ELISA (10 per group). Statistical significance was determined using Tukey's multiple-comparison test of one-way ANOVA (****, $P < 0.0001$). (E) IAV-infected mice were treated with isotype antibody (Ab) or anti-IFNAR1 blocking Ab at 6 h and 3 days postinfection. On day 6 postinfection, bone marrow cells were harvested from the indicated mice. Representative dot plots (left) and the percentage of GMP population (right) in mice treated with isotype Ab or anti-IFNAR1 blocking Ab are shown. Data from two independent experiments were combined ($n = 6$; means and SEM). Statistical significance was determined using the Student two-tailed t test (***, $P < 0.001$). (F and G) Naive B6 mice were treated with PBS or poly(I·C) via an intraperitoneal injection. On day 3 posttreatment, the bone marrow cells were harvested. The percentages of GMP population (F) and Ly6C$^+$ CCR2$^+$ monocytes (G) are shown. Data from two independent experiments were combined ($n = 6$; means and SEM). Statistical significance was determined using the Student two-tailed t test (***, $P < 0.001$).

blockage decreased GMP population expansion (Fig. 2E). To further support the idea that type I IFN plays an important role in the emergency expansion of the GMP population, poly(I·C), a double-stranded RNA mimic, was used to induce type I IFN in a noninfectious environment (17). As shown in Fig. 2F, the emergency expansion of the GMP population was significantly increased in poly(I·C)-treated mice compared with phosphate-buffered saline (PBS)-treated mice. Furthermore, the proportion of Ly6C$^+$ CCR2$^+$ monocytes in the bone marrow also increased after poly(I·C) treatment (Fig. 2G). Thus, these results revealed a novel functional role of type I IFN in the feedback regulation of emergency GMP population expansion and monopoiesis.

Upregulation of M-CSFR on bipotent GMPs and MPs was regulated by type I IFN. Next, we sought to further elucidate the mechanism underlying the type I IFN-mediated regulation of the GMP population expansion. Although a low expression of IFNAR1 has been detected in HSCs and MPPs, its expression in the GMP population is unknown (12). As shown in Fig. 3A, we demonstrated with uninfected and infected mice that IFNAR1 was expressed in the GMP population in both steady-state and demand-adapted hematopoiesis, suggesting that type I IFN may act directly on the GMP population. As bipotent GMPs can differentiate into MPs or GPs (31), we determined the M-CSFR expression on Ly6C$^-$ GMPs (bipotent GMPs) and Ly6C$^+$ GMPs (MPs/GPs) in uninfected and infected B6 mice. Compared with populations in uninfected mice, both M-CSFR$^+$ bipotent GMPs and MPs were increased in infected mice (Fig. 3B). Therefore, we focused on the impact of type I IFN on the regulation of M-CSFR expression in the GMP population. In the GMP population, the percentage of M-CSFR$^+$ GMPs was increased in infected B6 mice compared with uninfected mice, while the expansion of M-CSFR$^+$ GMPs was blocked in infected *Ifnar1*$^{-/-}$ mice and in infected WT mice administered anti-IFNAR antibody (Fig. 3C and D). As expected, M-CSFR expression in the GMP population was higher in mice treated with poly (I·C) than in PBS-treated mice (Fig. 3E). Only a sparse amount of G-CSFR protein (also known as CD114) was detected on cell surfaces (Fig. 3C), potentially due to the limited expression of G-CSFR per bipotent GMP or GP (32). The involvement of M-CSF expression in the emergency monopoiesis observed in this study was excluded, since there was no significant difference in the M-CSF expression between infected WT and *Ifnar1*$^{-/-}$ mice (see Fig. S1 in the supplemental material). In summary, we demonstrated that type I IFN is a potent inducer of M-CSFR$^+$ bipotent GMPs and MPs.

Type I IFN transcriptionally regulated M-CSFR expression via STAT1. Engagement of type I IFN with their receptors can activate the transcription factor STAT1 (14). To address whether STAT1 was required for M-CSFR expression, the mRNA expression of M-CSFR (also known as CSF1R) and G-CSFR (also known as CSF3R) in the sorted GMP populations of infected WT, *Ifnar1*$^{-/-}$, and *Stat1*$^{-/-}$ mice was measured. The mRNA expression of M-CSFR in the GMP population of infected *Ifnar1*$^{-/-}$ and *Stat1*$^{-/-}$ mice was only 40% of that in the GMP population of infected WT mice (Fig. 4A, left). Moreover, the mRNA expression of G-CSFR was not altered in either infected *Ifnar1*$^{-/-}$ or *Stat1*$^{-/-}$ mice compared with that in infected WT mice (Fig. 4A, right). Quantitative reverse transcription-PCR (qRT-PCR) (Fig. 4A) results demonstrated that G-CSFR expression in the GMP population was not regulated by the IFNAR1-STAT1 axis upon IAV infection.

To study the molecular mechanism of STAT1-mediated M-CSFR induction, reporter assays for M-CSFR promoter activity and chromatin immunoprecipitation (ChIP) assays for STAT1-DNA binding were performed. As shown in Fig. 4B, treatment of the monocytic RAW 264.7 cells with IFN-β induced the mRNA expression of M-CSFR. To explore whether STAT1 directly binds to the M-CSFR promoter and transactivates M-CSFR gene expression, a reporter plasmid with an M-CSFR promoter fragment spanning nucleotide positions -1335 to -26 was constructed. Based on sequence analysis, three potential STAT1 binding sites were predicted in this region of the M-CSFR promoter. Constructs with serial 5′ deletions in the promoter were generated to investigate the role of the putative STAT1 binding sites (Fig. 4C). As shown in Fig. 4D, an 8-fold increase in M-CSFR promoter activity was observed when IFN-β signaling was triggered. Based on the serial 5′ deletions of the M-CSFR promoter, the nucleotide sequence from -1205 to -1196 was essential for the type I IFN-mediated induction of M-CSFR expression. As shown in Fig. 4E, STAT1 was phosphorylated and activated in the presence of IFN-β. To confirm the binding of STAT1 to the endogenous M-CSFR promoter under physiological conditions, RAW 264.7 cells were treated with IFN-β and quantitative ChIP assays were performed. The results indicated that STAT1 bound to the M-CSFR promoter (Fig. 4F). In conclusion, these results demonstrated that type I IFN induced M-CSFR expression via the direct binding of STAT1 to the M-CSFR promoter, leading to the observed emergency monopoiesis upon IAV infection.

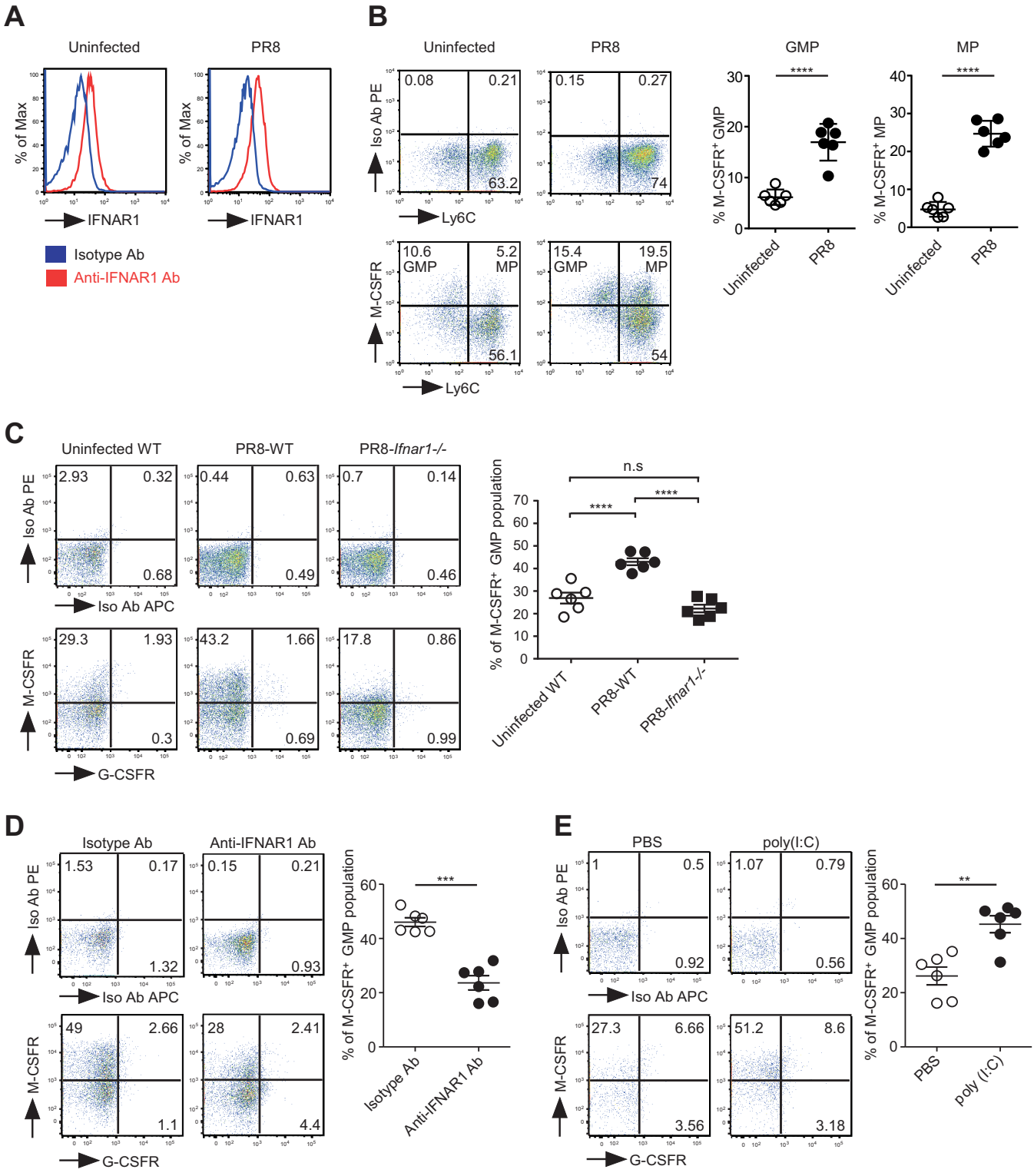

FIG 3 Type I IFN upregulated M-CSFR expression levels on bipotent GMPs and MPs. (A and B) Bone marrow cells were isolated from uninfected mice or on day 7 postinfection. (A) The expression of IFNAR1 on the GMP population was assayed by flow cytometry. (B) Percentages of M-CSFR$^+$ GMPs and M-CSFR$^+$ MPs. Statistical significance was determined using the Student two-tailed *t* test (****, $P < 0.0001$). Experiments were performed 4 times independently (means and SEM). (C) Bone marrow cells were harvested from infected WT and *Ifnar1*$^{-/-}$ mice on day 7 postinfection. The percentage of the M-CSFR$^+$ GMP population in indicated mice is shown. Results are representative of three repeated experiments with 6 mice per group (means and SEM). Statistical significance was determined using the Tukey's multiple-comparison test of one-way ANOVA (***, $P < 0.001$). (D) PR8-infected mice were treated with an isotype Ab or an anti-IFNAR1 blocking Ab at 6 h and 3 days postinfection. Bone marrow cells were harvested on day 6 postinfection. The percentage of the M-CSFR$^+$ GMP population is shown. Data from two independent experiments were combined ($n = 6$; means and SEM). Statistical significance was

(Continued on next page)

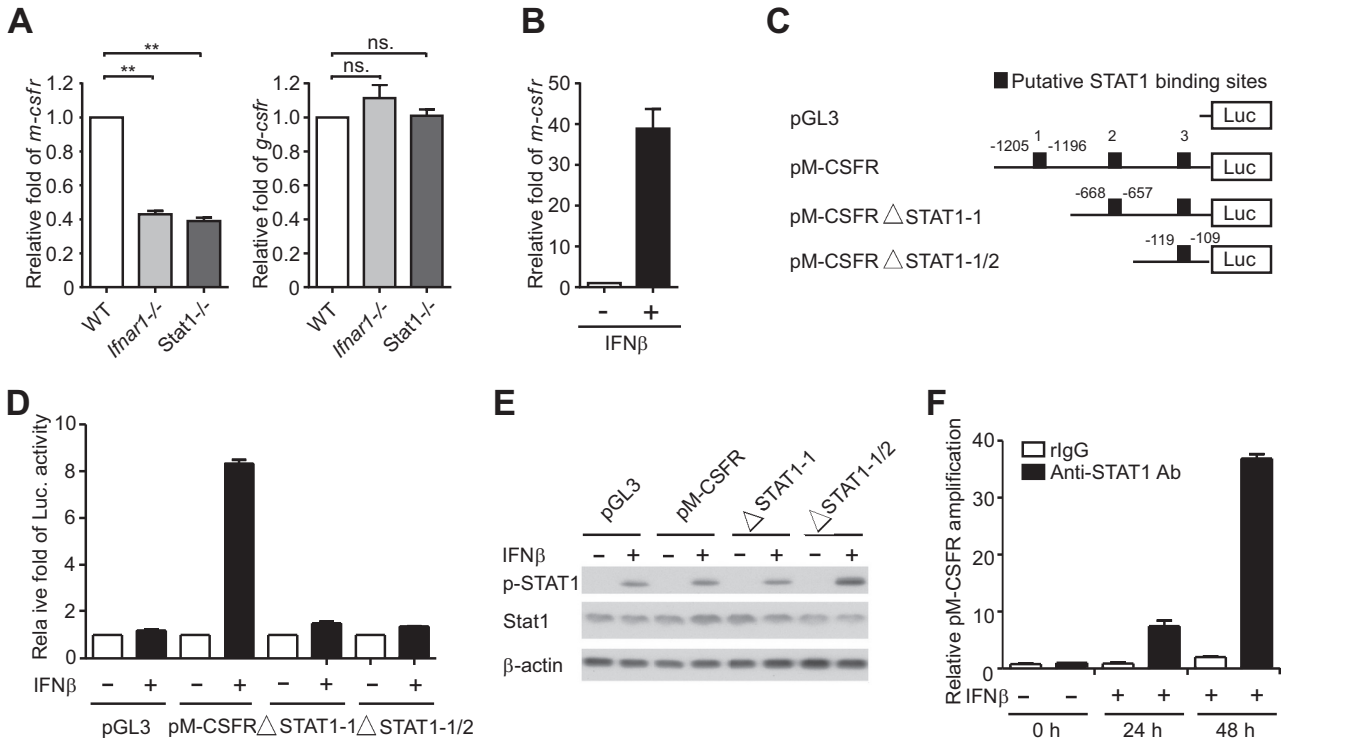

FIG 4 STAT1 upregulated the expression of M-CSFR gene. (A) WT, *Ifnar1*$^{-/-}$, and *Stat1*$^{-/-}$ mice were infected with PR8 viruses. Bone marrow cells were harvested on day 7 postinfection. The relative expression levels of transcripts of M-CSFR (left) and G-CSFR (right) in the sorted GMP population were assayed by qRT-PCR. The relative fold expression was compared to that in the WT group after normalization with GAPDH expression. A representative result is shown (4 to 6 per group; means and SEM) (ns, no significant difference; **, $P < 0.01$). The experiments were performed 3 times independently. (B) The M-CSFR mRNA expression levels in RAW 264.7 cells were examined by qRT-PCR before and after IFN-β treatment. The relative fold expression was compared to that of the untreated group after normalization to GAPDH expression. The experiments were performed twice independently. (C) A schematic illustration of the M-CSFR promoter that drives the luciferase gene in the reporter plasmid is shown; three putative STAT1-binding sites are indicated. (D and E) The relative luciferase activities (D) and phosphorylation of STAT1 (E) between untreated and IFN-β-treated RAW 264.7 cells are shown. (F) M-CSFR promoter (pM-CSFR) DNA was detected in STAT1 pulldown immunoprecipitates by qPCR. The relative fold amplification of pM-CSFR at 24 and 48 h post-IFN-β treatment was compared to that of the untreated group.

Knockout of STAT1 blocked emergency monopoiesis and enhanced bacterial clearance in IAV-infected mice. As shown in Fig. 5A, we demonstrated that the IAV-induced GMP population expansion was reduced in infected *Stat1*$^{-/-}$ mice. Furthermore, the upregulation of M-CSFR expression in the GMP population was not observed in infected *Stat1*$^{-/-}$ mice compared with infected WT mice (Fig. 5B). These results indicated that type I IFN-IFNAR1 signaling triggered the expansion of the GMP population and the induction of M-CSFR expression in a STAT1-dependent manner.

IAV infection followed by secondary bacterial pneumonia has been reported to result in increased mortality. *Streptococcus pneumoniae*, *Staphylococcus aureus*, and *Klebsiella pneumoniae* are the most common causes of IAV-mediated secondary bacterial pneumonia (22). Previous studies have demonstrated that type I IFN and poly(I·C) impair the clearance of IAV-mediated secondary bacterial infections (18–20, 33). However, the mechanism by which IAV sensitizes hosts to secondary bacterial infections remains unclear. To address the potential impact of type I IFN-induced emergency monopoiesis on IAV-mediated secondary bacterial infection, *S. pneumoniae* was used to challenge IAV-infected WT and *Stat1*$^{-/-}$ mice. Compared with WT mice, *Stat1*$^{-/-}$ mice presented fewer infiltrating monocytes and more infiltrating granulocytes in the lungs (Fig. 5C). Importantly, *Stat1*$^{-/-}$ mice effectively eliminated secondary bacterial infection (Fig. 5D).

FIG 3 Legend (Continued)
determined using the Student two-tailed *t* test (***, $P < 0.001$). (E) Naive B6 mice were treated with PBS or poly(I·C) via an intraperitoneal injection. On day 3 posttreatment, the bone marrow cells were harvested from mice. The percentage of the M-CSFR^{+} GMP population was shown. Data from two independent experiments were combined ($n = 6$; means and SEM). Statistical significance was determined using the Student two-tailed *t* test (**, $P < 0.01$).

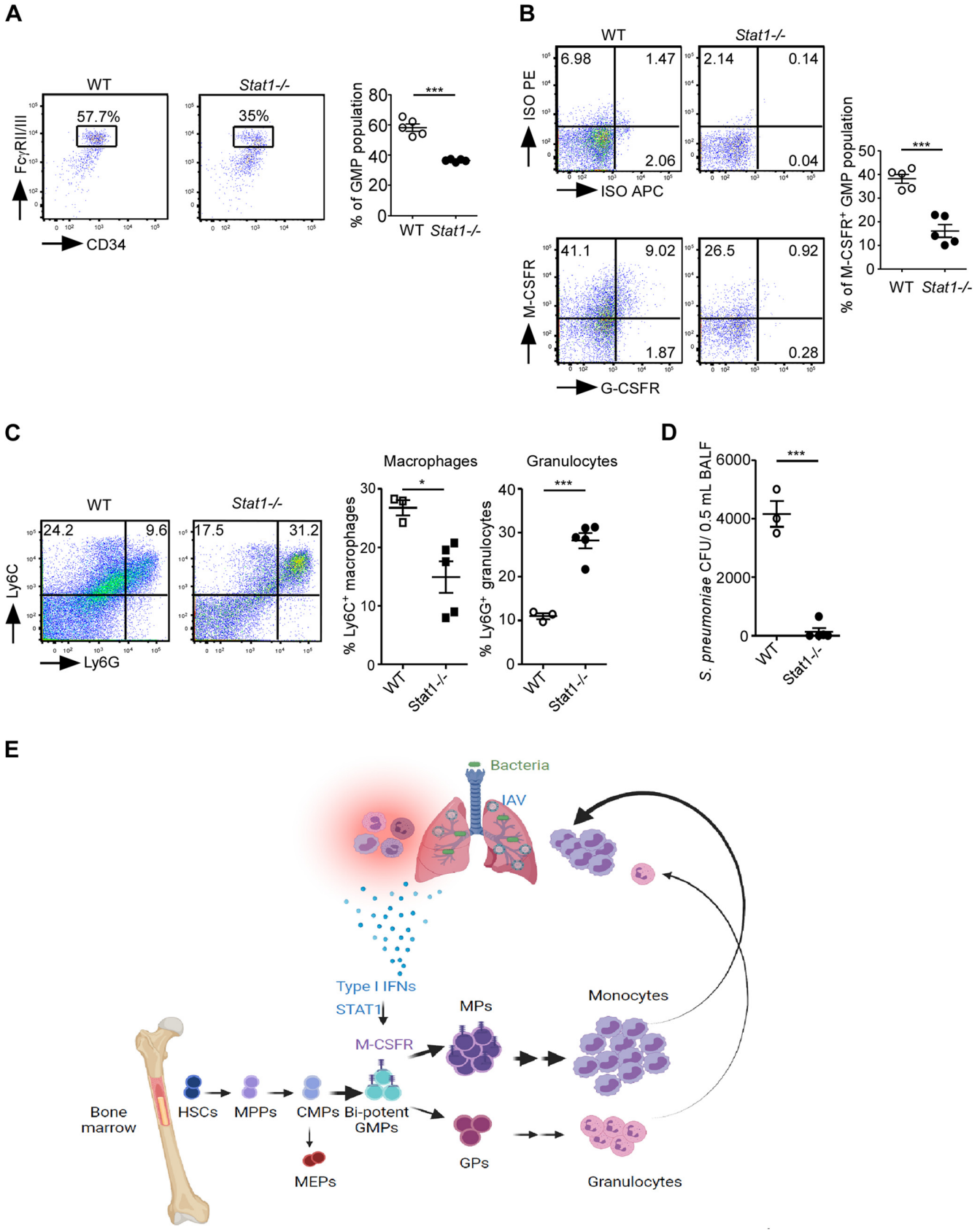

FIG 5 Impaired demanding monopoiesis accelerated bacterial clearance in IAV-infected mice. WT and *Stat1*$^{-/-}$ mice were infected with PR8 viruses. Bone marrow cells were harvested on day 7 postinfection. (A and B) Percentages of GMP population (A) and M-CSFR^{+} GMP population (B) for the indicated

(Continued on next page)

In Fig. 5E, we model our findings, as follows. Type I IFN is initially induced and results in the preferential infiltration of bone marrow-derived Ly6C$^+$ CCR2$^+$ monocytes. The RLR–IPS-1 axis of the infiltrating Ly6C$^+$ CCR2$^+$ monocyte-derived cells is also triggered to increase the production of type I IFN. The expansion of the GMP population then results from hematopoiesis shifting from a steady state to an emergency status via type I IFN-IFNAR1 signaling in a STAT1-dependent manner. In the GMP population, type I IFN binds to IFNAR1 to activate STAT1, which in turn binds to the M-CSFR promoter, leading to increased expression of the M-CSFR gene. The more M-CSFR-expressing bipotent GMPs and MPs are generated, the more monocytes are produced to be potentially recruited to the site of infection. Therefore, a positive regulatory feedback loop mediated by type I IFN is established. At the same time, a decreased proportion of granulocytes are produced as a result of the emergency monopoiesis, possibly contributing to increased host susceptibility to secondary bacterial infections. This model provides a novel insight into how type I IFN orchestrates monopoiesis to achieve a balance between the supply and demand of monocytes during IAV infection but may compromise bacterial clearance ability of IAV-infected hosts during secondary bacterial infection and increase the risk of a negative disease outcome.

DISCUSSION

Monocytes and granulocytes are the first line of defense against pathogen invasion; however, they are rapidly consumed during infection due to their short half-life (1, 2). To replenish the pool of monocytes and granulocytes, different adaptations of myelopoiesis have been found in response to different pathogen invasions, including systemic and local infections. Sepsis, a systemic infection, activates B cells to secrete IL-3, resulting in emergency myelopoiesis of Ly6C$^+$ monocytes and granulocytes (34). Systemic infection with *Listeria monocytogenes* selectively promotes TLR signaling-dependent monopoiesis (35). Local mycobacterial infection alters hematopoiesis in the bone marrow and lungs. For example, *Mycobacterium tuberculosis* induces the accumulation of bone marrow-derived Ly6C$^+$ monocytes followed by their expansion *in situ* (36). Moreover, *Toxoplasma gondii* infection causes natural killer cell-derived IFN-γ to prime CMPs, leading to an increase in Ly6C$^+$ monocyte generation (37). In severe respiratory viral infections, while the accumulation of Ly6C$^+$ monocytes/macrophages in the lungs has been found to be a predominant phenomenon (7, 8, 25, 28), the homeostasis of monocytes in the bone marrow remains unknown.

Monocytes are produced in the bone marrow from two independent progenitors: bipotent GMPs and MDPs (10). In our IAV infection model, the MDP population was only slightly increased after infection (Fig. S2), which is consistent with a previous IAV infection study (5). Meanwhile, the GMP population was dramatically scaled up (Fig. 1G and H). We further demonstrated that type I IFN plays an important role in regulating the expansion of the GMP population but is not involved in its upstream HSCs (Fig. 1). These results suggest that type I IFN not only regulates a precise adaptation to meet the additional need of monocytes/macrophages in the periphery but also provides a mechanism to prevent HSC exhaustion in the bone marrow during IAV infection.

Several lines of evidence indicate that infection with IAV strains of higher pathogenicity is associated with higher levels and prolonged expression of type I IFN (7, 22). We found that the expansion of the GMP population is dependent on the magnitude of type I IFN expression (Fig. S3). Moreover, consistent with a previous study (15), we could not detect IAV in the bone marrow by qRT-PCR and plaque assays (data not

FIG 5 Legend (Continued)
mice. Results are representative of three similar experiments with five mice per group (means and SEM). (C) Percentages of Ly6C$^+$ macrophages and Ly6G$^+$ granulocytes in IAV- and *Streptococcus pneumoniae*-coinfected WT and *Stat1*$^{-/-}$ mice. Results are representative of three similar experiments with 3 to 5 mice per group (means and SEM). (D) Bacterial loads in IAV- and *S. pneumoniae*-coinfected WT and *Stat1*$^{-/-}$ mice. Results are representative of three similar experiments with 3 to 5 mice per group (means and SEM). Statistical significance was determined using the Student two-tailed *t* test (*, $P < 0.05$; ***, $P < 0.001$). (E) Model showing the impact of type I IFNs on the shift of monopoiesis from a steady state toward a demand-adapted state upon IAV infection.

shown). Our findings indicate that a strong and prolonged type I IFN exposure leads to a hematopoietic shift from steady-state to demand-adapted monopoiesis.

Previous studies have consistently shown that type I IFN is a detrimental factor contributing to the development of IAV-induced secondary bacterial infection that occurs 3 to 7 days postinfection (18, 22). Treatment with poly(I·C), which induces type I IFN without causing tissue damage, also sensitizes IAV-infected hosts to secondary bacterial infection (33). Furthermore, chronic type I IFN treatment often leads to neutropenia and causes infectious complications in the clinic (38). In this study, we found that IAV-infected *Stat1*$^{-/-}$ mice did not exhibit demand-adapted monopoiesis, showed a reduction in monocyte influx and enrichment of granulocyte recruitment, and had decreased bacterial burden (Fig. 5). Therefore, type I IFN plays a critical role not only in controlling the ratio of MPs and GPs generated in bone marrow but also in regulating the recruitment of monocytes and granulocytes in the inflamed lungs. This type I IFN-mediated positive feedback loop of monocyte infiltration and production between the lungs and the bone marrow plays a pivotal role in replenishing depleted monocytes during IAV infection but also potentially in the development of IAV-associated secondary bacterial infections. Our study thus provides important insights into mechanisms by which respiratory viral infection may increase susceptibility to secondary bacterial invasion. Future research should focus on the fine-tuning of demand-adapted monopoiesis to counteract the detrimental effect of type I IFN on respiratory viral-bacterial coinfections.

MATERIALS AND METHODS

Mouse strains. C57BL/6J (B6; wild-type, WT) and gene-deficient strains of *Stat1*$^{-/-}$ mice were purchased from The Jackson Laboratory (Bar Harbor, ME, USA). B6.SJL (Ly5.1) congenic mice were purchased from Taconic (Rensselaer, NY, USA). *Ips-1*$^{-/-}$ mice were provided by Michael Gale, Jr. Sources of *Ifnar1*$^{-/-}$ and *Myd88*$^{-/-}$ mice were described previously (7). The mice were kept under specific-pathogen-free (SPF) conditions in a biosafety level 2 (BSL-2) facility. All animal protocols were approved by the Institutional Animal Care and User Committee of National Taiwan University.

Virus preparation and inoculation. H1N1 A/Puerto Rico/8/34 (PR8) was propagated in SPF 10-day-old embryonated chicken eggs. Harvested viruses were aliquoted, titrated by plaque assay, and stored at −80°C until use. For IAV inoculation, adult mice were intranasally infected with 200 PFU of viruses.

Collection of BALF and determination of IFN-β expression by ELISA. To obtain BALF, mouse airways were flushed three times with sterile PBS (0.5 mL) and centrifuged to remove the cells. The expression of IFN-β in the BALF of the indicated mice was measured using the mouse IFN-β enzyme-linked immunosorbent assay (ELISA) kit (Life Technologies, Carlsbad, CA, USA), according to the manufacturer's instructions.

Leukocyte preparation from the lungs, MLNs, spleen, and bone marrow. Harvested lungs were homogenized using a metal mesh, and the suspension was treated with 600 U of type I collagenase (Invitrogen, Carlsbad, CA, USA) for 40 min at 37°C. The femurs and tibiae were harvested, and bone marrow cells were flushed out with RPMI medium by inserting a 1-mL syringe with a 26-gauge needle into one end of the bone. MLNs and spleens were homogenized using glass slides with ground edges. Leukocytes isolated from the lungs, MLNs, spleen, and bone marrow were obtained after red blood cell (RBC) lysis buffer treatment, and the cells were washed once with complete RPMI medium containing 10% fetal calf serum (FCS), 1 mM glutamine, 100 U/mL of penicillin, and 100 μg/mL of streptomycin.

Immunofluorescent surface staining. Two million cells were stained with fluorescently labeled monoclonal antibodies for 30 min at 4°C. Fluorescently labeled antibodies against Gr1 (clone RB6-8C5; eBioscience, San Diego, CA, USA), CD11b (clone M1/70; BD Biosciences, Franklin Lakes, NJ, USA), Ly6C (clone AL-21; BD Biosciences), Ly6G (clone1A8; eBioscience), Ly5.1 (clone A20; eBioscience), IL-7Rα (clone A7R34; eBioscience), c-Kit (clone 2B8; eBioscience), Sca-1 (clone D7; BD Biosciences), FcγRII/RIII (clone 2.4G2; BD Biosciences), CD34 (clone RAM34; eBioscience), IFNAR1 (clone MAR1-5A3; eBioscience), M-CSFR (rat antibody; R&D Systems, Inc.), G-CSFR (clone 723806; R&D Systems, Inc.), CCR2 (rat antibody; R&D Systems, Inc.), and a hematopoietic lineage cocktail (containing anti-mouse CD3, anti-mouse B220, anti-mouse CD11b, anti-mouse TER-119, and anti-mouse Gr1; eBioscience) were used in this study. After staining, the cells were fixed with Cytofix (BD Biosciences) for 5 min at 4°C. Finally, the cells were washed and resuspended in PBS with 2% FCS and analyzed by flow cytometry (BD Biosciences). HSPCs were identified according to the expression levels of surface markers as described in previous studies (10, 27): LSK cells (IL-7Rα^- Lin$^-$ Sca-1$^+$ c-Kit$^+$), CMPs (IL-7Rα^- Lin$^-$ Sca-1$^-$ c-Kit$^+$ FcγRII/III^{low} CD34$^+$), GMPs (IL-7Rα^- Lin$^-$ Sca-1$^-$ c-Kit$^+$ FcγRII/III^{high} CD34$^+$), MPs (IL-7Rα^- Lin$^-$ Sca-1$^-$ c-Kit$^+$ FcγRII/III^{high} CD34$^+$ CD115$^+$ Ly6C$^+$), GPs (IL-7Rα^- Lin$^-$ Sca-1$^-$ c-Kit$^+$ FcγRII/III^{high} CD34$^+$ CD115$^-$ Ly6C$^+$), and MEPs (IL-7Rα^- Lin$^-$ Sca-1$^-$ c-Kit$^+$ FcγRII/III$^-$ CD34$^-$).

Adoptive transfer of Ly5.1$^+$ GMP population into Ly5.2 mice. Bone marrow cells were harvested from Ly5.1 mice at day 5 postinfection, and HSPCs were purified using the EasySep mouse hematopoietic cell isolation kit (STEMCELL Technologies, Vancouver, BC, Canada). Isolated HSPCs were stained with fluorescently labeled antibodies, including c-Kit, Sca-1, FcγRII/III, and CD34. The c-Kit$^+$ Sca-1$^-$ FcγRII/III^{high} CD34$^+$ GMP population was sorted using a cell sorter (BD FACSAria II), and then the GMP

population was suspended in PBS at a concentration of 1×10^6 cells/mL. Ten thousand cells of the GMP population were adoptively transferred via the tail vein into Ly5.2 mice at day 1 postinfection. Bone marrow cells were harvested on day 6 postinfection, and cells were stained with antibodies against Ly5.1, Gr1, CD11b, Ly6C, and CCR2 molecules. Finally, the transferred Ly5.1$^+$ cells were further analyzed for Gr1$^+$ CD11b$^+$ myeloid cells and Ly6C$^+$ CCR2$^+$ monocytes.

Poly(I·C) treatment. Naive B6 mice were injected intraperitoneally with 125 μg/mouse poly(I·C) (GE Healthcare Life Sciences, Chicago, IL, USA) or PBS alone. Bone marrow cells were harvested on day 3 posttreatment.

Anti-IFNAR1 blocking antibody treatment. Mice were injected intraperitoneally with 150 μg/mouse isotype IgG control antibody (Abcam, Cambridge, UK) or 150 μg/mouse anti-IFNAR1 blocking antibody (clone MAR1-5A3; eBioscience) twice, at 6 h and 3 days postinfection. Bone marrow cells were harvested on day 6 postinfection.

RNA extraction and qRT-PCR. Leukocytes were isolated from the lungs as previously described (7). Leukocytes were stained with antibodies against Gr1, CD11b, Ly6C, and CCR2 molecules, and then infiltrating Ly6C$^+$ CCR2$^+$ monocytes/macrophages were sorted out from the indicated mice. The GMP population was sorted from the bone marrow of infected WT, *Ifnar1*$^{-/-}$, and *Stat1*$^{-/-}$ mice on day 7 postinfection. RAW 264.7 cells were treated with or without IFN-β for 48 h. Total RNA was extracted from sorted Ly6C$^+$ CCR2$^+$ monocytes, sorted GMP populations of indicated mice, and RAW 264.7 cells, using TRIzol reagent (Invitrogen) according to the manufacturer's instructions. One microgram of RNA was used to synthesize cDNA using Superscript III reverse transcriptase (Invitrogen). TaqMan gene expression assays (Applied Biosystems, Waltham, MA, USA) were performed to detect mouse transcripts of M-CSFR (assay ID, Mm01266652_m1), G-CSFR (assay ID, Mm00432735_m1), IFN-β (assay ID, Mm00439552_s1), and glyceraldehyde 3-phosphate dehydrogenase (GAPDH) (assay ID, Mm99999915_g1). Relative gene expression was determined using cycle threshold ($\Delta\Delta C_T$) analysis. Briefly, expression of the various genes was normalized to the GAPDH level in each group, and the resulting level of the indicated transcripts in WT mice or untreated RAW 264.7 cells was set as 1 to calculate the relative level (fold) of the transcripts in knockout mice or IFN-β-treated RAW 264.7 cells.

Reporter assay of the M-CSFR promoter. A series of luciferase reporter plasmids driven from M-CSFR promoter fragments (nucleotides [nt] −1335 to −26 [pM-CSFR], nt −829 to −26 [pM-CSFR△STAT1-1]), and nt −416 to −26 (pM-CSFR△STAT1-1/2) were inserted into the pGL3-basic vector (Promega, Madison, WI, USA) through the HindIII and XhoI sites. Primers for pM-CSFR were as follows: pM-CSFR forward, 5′-CCGCTCGAGCGGGCATTACACGTATGTGCACC; pM-CSFR△STAT1-1, forward XhoI, 5′-CCGCTCGAGCGGAGGC AGGAACAGACTTGAAG; pM-CSFR△STAT1-1/2, forward XhoI, 5′-CCGCTCGAGCGGATCTCCAGTTACCTTGAGGC; and common reverse HindIII, 5′-CCCAAGCTTGGGGATGAACACGTTCCTGTCTG-3′. RAW 264.7 cells were seeded at a density of 2×10^5 cells/well in a 12-well plate and then transfected with 1 μg of pGL3 or various *m-csfr* promoter–luciferase reporter plasmids combined with 0.2 μg green fluorescent protein (GFP)-expressing plasmids (pEGFP-C1; Promega) using Lipofectamine 2000 (Invitrogen) according to the manufacturer's instructions. After 48 h, transfected cells were treated with 100 ng/mL of mouse IFN-β (Peprotech, Rocky Hill, NJ, USA) for another 48 h. Luciferase activity and GFP fluorescence intensity were detected using the Bright-Glo luciferase assay system kit (Promega). The relative fold induction of luciferase activity from each transfectant was normalized to its GFP intensity and standardized with untreated RAW 264.7 cell control.

ChIP assay. RAW 264.7 cells were treated with 100 ng/mL IFN-β for 24 or 48 h. The Pierce magnetic ChIP kit (Thermo Fisher Scientific, Inc., Waltham, MA, USA) was used to extract STAT1-binding DNA. STAT1-bound DNA was analyzed by quantitative PCR with primers targeting the M-CSFR promoter (pM-CSFR from nt −1147 to −1256) as follows: forward, 5′-CGAACCTAGGTCCTCTGCAA-3′, and reverse, 5′-TTGGGGATCTCTAGCCCTTT-3′. Quantitative PCR was performed using the SensiFAST SYBR No-ROX kit (Bioline, London, UK) and CFX Connect real-time PCR detection system (Bio-Rad, Hercules, CA, USA). Polymerase was activated at 95°C for 2 min. Thirty-nine cycles of 95°C for 5 s, 60°C for 10 s, and 72°C for 15 s were performed t to amplify the targeted pM-CSFR sequence.

Western blotting. RAW 264.7 cells were treated with 100 ng/mL of IFN-β for 24 or 48 h, and the cells were lysed using radioimmunoprecipitation assay buffer (50 mM Tris [pH 7.5], 150 mM sodium chloride, 1% Nonidet P-40, 1% sodium deoxycholate, and 0.1% sodium dodecyl sulfate [SDS] with protease inhibitors). Cell lysates were resolved by electrophoresis on SDS-polyacrylamide gels and electrotransferred onto Hybond-C Extra membranes (Amersham Biosciences, Piscataway, NJ, USA). Milk-blocked blots were incubated with primary antibodies against phosphorylated STAT1 (Cell Signaling Technology), anti-STAT1 (Cell Signaling Technology), and anti-β-actin (clone AC-15; Sigma, St. Louis, MO, USA) at 4°C overnight and then washed and incubated with horseradish peroxidase-conjugated secondary antibodies (Jackson ImmunoResearch, Baltimore, MD, USA) at room temperature for 1 h. The proteins of interest were visualized using Western Lightning chemiluminescence reagent (PerkinElmer Life Sciences, Boston, MA, USA).

***S. pneumoniae* challenge and determination of CFU in BALFs.** A type 2 D39 *S. pneumoniae* strain was obtained from Yung-Chiy Chang (Graduate Institute of Microbiology, College of Medicine, National Taiwan university, Taipei, Taiwan). Bacteria were grown in yeast extract containing Todd-Hewitt broth at 37°C and 5% carbon dioxide (CO_2) for 6 h. The concentration of bacteria was measured by determining the optical density (OD) at 600 nm, and then the number of CFU was calculated (1 OD unit = 1×10^8 CFU). WT and *Stat1*$^{-/-}$ mice were infected with 200 PFU of PR8 virus. On day 6 postinfection, virus-infected mice were further challenged with 1×10^7 CFU of *S. pneumoniae*. Bacterial loads and the percentages of Ly6C$^+$ macrophages and Ly6G$^+$ granulocytes in BALF were measured 24 h after secondary *S. pneumoniae* infection. To obtain BALF, the mouse airway was flushed three times 0.5 mL sterile PBS. Collected BALFs were 10-fold serially diluted with PBS and plated on blood agar (BD Biosciences). The number of CFU of *S. pneumoniae* was calculated after overnight incubation at 37°C in a 5% CO_2

incubator. Ly6C$^+$ macrophages and Ly6G$^+$ granulocytes in BALF were stained with antibodies against Ly6C and Ly6G.

Statistics. The statistical significance of data was analyzed using GraphPad Prism software by the Student two-tailed *t* test or by Tukey's multiple-comparison test of one-way analysis of variance (ANOVA).

Data availability. All data are available in the text and in the supplemental material.

SUPPLEMENTAL MATERIAL

Supplemental material is available online only.

SUPPLEMENTAL FILE 1, PDF file, 0.1 MB.

ACKNOWLEDGMENTS

This work was supported by the Excellent Translational Medicine Research Projects of National Taiwan University College of Medicine, National Taiwan University Hospital (105R39012), the National Health Research Institute (NHRI-EX107-10735SI, NHRI-EX108-10735SI, and NHRI-EX109-10735SI), and the National Science and Technology Council (109-2320-B-002-052-MY3).

We thank Editage (www.editage.com) for English language editing.

S.-J.L. designed and performed the experiments, analyzed the data, and cowrote the manuscript; K.-M.L. performed the experiments, analyzed the data, and cowrote the manuscript; S.-Y.C. cowrote the manuscript; C.-C.K. performed the experiments and provided materials; C.-W.H. and C.-H.H. performed the experiments; M.G. provided *Ips-1* knockout mice; and C.-H.T. designed the experiments and cowrote the manuscript.

We declare that we have no competing financial interests.

REFERENCES

1. Schultze JL, Mass E, Schlitzer A. 2019. Emerging principles in myelopoiesis at homeostasis and during infection and inflammation. Immunity 50:288–301. https://doi.org/10.1016/j.immuni.2019.01.019.
2. Manz MG, Boettcher S. 2014. Emergency granulopoiesis. Nat Rev Immunol 14:302–314. https://doi.org/10.1038/nri3660.
3. Ghoneim HE, Thomas PG, McCullers JA. 2013. Depletion of alveolar macrophages during influenza infection facilitates bacterial superinfections. J Immunol 191:1250–1259. https://doi.org/10.4049/jimmunol.1300014.
4. McGill J, Van Rooijen N, Legge KL. 2008. Protective influenza-specific CD8 T cell responses require interactions with dendritic cells in the lungs. J Exp Med 205:1635–1646. https://doi.org/10.1084/jem.20080314.
5. Beshara R, Sencio V, Soulard D, Barthelemy A, Fontaine J, Pinteau T, Deruyter L, Ismail MB, Paget C, Sirard JC, Trottein F, Faveeuw C. 2018. Alteration of Flt3-ligand-dependent de novo generation of conventional dendritic cells during influenza infection contributes to respiratory bacterial superinfection. PLoS Pathog 14:e1007360. https://doi.org/10.1371/journal.ppat.1007360.
6. Stifter SA, Bhattacharyya N, Pillay R, Florido M, Triccas JA, Britton WJ, Feng CG. 2016. Functional interplay between type I and II interferons is essential to limit influenza A virus-induced tissue inflammation. PLoS Pathog 12:e1005378. https://doi.org/10.1371/journal.ppat.1005378.
7. Lin SJ, Lo M, Kuo RL, Shih SR, Ojcius DM, Lu J, Lee CK, Chen HC, Lin MY, Leu CM, Lin CN, Tsai CH. 2014. The pathological effects of CCR2+ inflammatory monocytes are amplified by an IFNAR1-triggered chemokine feedback loop in highly pathogenic influenza infection. J Biomed Sci 21:99. https://doi.org/10.1186/s12929-014-0099-6.
8. Lin KL, Suzuki Y, Nakano H, Ramsburg E, Gunn MD. 2008. CCR2+ monocyte-derived dendritic cells and exudate macrophages produce influenza-induced pulmonary immune pathology and mortality. J Immunol 180:2562–2572. https://doi.org/10.4049/jimmunol.180.4.2562.
9. Boettcher S, Manz MG. 2017. Regulation of inflammation- and infection-driven hematopoiesis. Trends Immunol 38:345–357. https://doi.org/10.1016/j.it.2017.01.004.
10. Yanez A, Coetzee SG, Olsson A, Muench DE, Berman BP, Hazelett DJ, Salomonis N, Grimes HL, Goodridge HS. 2017. Granulocyte-monocyte progenitors and monocyte-dendritic cell progenitors independently produce functionally distinct monocytes. Immunity 47:890–902.E4. https://doi.org/10.1016/j.immuni.2017.10.021.
11. Zhao JL, Ma C, O'Connell RM, Mehta A, DiLoreto R, Heath JR, Baltimore D. 2014. Conversion of danger signals into cytokine signals by hematopoietic stem and progenitor cells for regulation of stress-induced hematopoiesis. Cell Stem Cell 14:445–459. https://doi.org/10.1016/j.stem.2014.01.007.
12. Takizawa H, Boettcher S, Manz MG. 2012. Demand-adapted regulation of early hematopoiesis in infection and inflammation. Blood 119:2991–3002. https://doi.org/10.1182/blood-2011-12-380113.
13. King KY, Goodell MA. 2011. Inflammatory modulation of HSCs: viewing the HSC as a foundation for the immune response. Nat Rev Immunol 11:685–692. https://doi.org/10.1038/nri3062.
14. Ivashkiv LB, Donlin LT. 2014. Regulation of type I interferon responses. Nat Rev Immunol 14:36–49. https://doi.org/10.1038/nri3581.
15. Hermesh T, Moltedo B, Moran TM, Lopez CB. 2010. Antiviral instruction of bone marrow leukocytes during respiratory viral infections. Cell Host Microbe 7:343–353. https://doi.org/10.1016/j.chom.2010.04.006.
16. Gough DJ, Messina NL, Clarke CJ, Johnstone RW, Levy DE. 2012. Constitutive type I interferon modulates homeostatic balance through tonic signaling. Immunity 36:166–174. https://doi.org/10.1016/j.immuni.2012.01.011.
17. Essers MA, Offner S, Blanco-Bose WE, Waibler Z, Kalinke U, Duchosal MA, Trumpp A. 2009. IFNalpha activates dormant haematopoietic stem cells in vivo. Nature 458:904–908. https://doi.org/10.1038/nature07815.
18. Shahangian A, Chow EK, Tian X, Kang JR, Ghaffari A, Liu SY, Belperio JA, Cheng G, Deng JC. 2009. Type I IFNs mediate development of postinfluenza bacterial pneumonia in mice. J Clin Invest 119:1910–1920. https://doi.org/10.1172/JCI35412.
19. Nakamura S, Davis KM, Weiser JN. 2011. Synergistic stimulation of type I interferons during influenza virus coinfection promotes Streptococcus pneumoniae colonization in mice. J Clin Invest 121:3657–3665. https://doi.org/10.1172/JCI57762.
20. Lee B, Robinson KM, McHugh KJ, Scheller EV, Mandalapu S, Chen C, Di YP, Clay ME, Enelow RI, Dubin PJ, Alcorn JF. 2015. Influenza-induced type I interferon enhances susceptibility to gram-negative and gram-positive bacterial pneumonia in mice. Am J Physiol Lung Cell Mol Physiol 309:L158–67. https://doi.org/10.1152/ajplung.00338.2014.
21. Boxx GM, Cheng G. 2016. The roles of type I interferon in bacterial infection. Cell Host Microbe 19:760–769. https://doi.org/10.1016/j.chom.2016.05.016.
22. McCullers JA. 2014. The co-pathogenesis of influenza viruses with bacteria in the lung. Nat Rev Microbiol 12:252–262. https://doi.org/10.1038/nrmicro3231.

23. Rynda-Apple A, Robinson KM, Alcorn JF. 2015. Influenza and bacterial superinfection: illuminating the immunologic mechanisms of disease. Infect Immun 83:3764–3770. https://doi.org/10.1128/IAI.00298-15.
24. Sun K, Metzger DW. 2008. Inhibition of pulmonary antibacterial defense by interferon-gamma during recovery from influenza infection. Nat Med 14:558–564. https://doi.org/10.1038/nm1765.
25. Seo SU, Kwon HJ, Ko HJ, Byun YH, Seong BL, Uematsu S, Akira S, Kweon MN. 2011. Type I interferon signaling regulates Ly6C(hi) monocytes and neutrophils during acute viral pneumonia in mice. PLoS Pathog 7:e1001304. https://doi.org/10.1371/journal.ppat.1001304.
26. Perrone LA, Plowden JK, Garcia-Sastre A, Katz JM, Tumpey TM. 2008. H5N1 and 1918 pandemic influenza virus infection results in early and excessive infiltration of macrophages and neutrophils in the lungs of mice. PLoS Pathog 4:e1000115. https://doi.org/10.1371/journal.ppat.1000115.
27. Yanez A, Ng MY, Hassanzadeh-Kiabi N, Goodridge HS. 2015. IRF8 acts in lineage-committed rather than oligopotent progenitors to control neutrophil vs monocyte production. Blood 125:1452–1459. https://doi.org/10.1182/blood-2014-09-600833.
28. Aldridge JR, Jr, Moseley CE, Boltz DA, Negovetich NJ, Reynolds C, Franks J, Brown SA, Doherty PC, Webster RG, Thomas PG. 2009. TNF/iNOS-producing dendritic cells are the necessary evil of lethal influenza virus infection. Proc Natl Acad Sci U S A 106:5306–5311. https://doi.org/10.1073/pnas.0900655106.
29. Kawai T, Takahashi K, Sato S, Coban C, Kumar H, Kato H, Ishii KJ, Takeuchi O, Akira S. 2005. IPS-1, an adaptor triggering RIG-I- and Mda5-mediated type I interferon induction. Nat Immunol 6:981–988. https://doi.org/10.1038/ni1243.
30. Kato H, Sato S, Yoneyama M, Yamamoto M, Uematsu S, Matsui K, Tsujimura T, Takeda K, Fujita T, Takeuchi O, Akira S. 2005. Cell type-specific involvement of RIG-I in antiviral response. Immunity 23:19–28. https://doi.org/10.1016/j.immuni.2005.04.010.
31. Rieger MA, Hoppe PS, Smejkal BM, Eitelhuber AC, Schroeder T. 2009. Hematopoietic cytokines can instruct lineage choice. Science 325:217–218. https://doi.org/10.1126/science.1171461.
32. McKinstry WJ, Li CL, Rasko JE, Nicola NA, Johnson GR, Metcalf D. 1997. Cytokine receptor expression on hematopoietic stem and progenitor cells. Blood 89:65–71. https://doi.org/10.1182/blood.V89.1.65.
33. Tian X, Xu F, Lung WY, Meyerson C, Ghaffari AA, Cheng G, Deng JC. 2012. Poly I:C enhances susceptibility to secondary pulmonary infections by gram-positive bacteria. PLoS One 7:e41879. https://doi.org/10.1371/journal.pone.0041879.
34. Weber GF, Chousterman BG, He S, Fenn AM, Nairz M, Anzai A, Brenner T, Uhle F, Iwamoto Y, Robbins CS, Noiret L, Maier SL, Zonnchen T, Rahbari NN, Scholch S, Klotzsche-von Ameln A, Chavakis T, Weitz J, Hofer S, Weigand MA, Nahrendorf M, Weissleder R, Swirski FK. 2015. Interleukin-3 amplifies acute inflammation and is a potential therapeutic target in sepsis. Science 347:1260–1265. https://doi.org/10.1126/science.aaa4268.
35. Serbina NV, Hohl TM, Cherny M, Pamer EG. 2009. Selective expansion of the monocytic lineage directed by bacterial infection. J Immunol 183:1900–1910. https://doi.org/10.4049/jimmunol.0900612.
36. Huang L, Nazarova EV, Tan S, Liu Y, Russell DG. 2018. Growth of Mycobacterium tuberculosis in vivo segregates with host macrophage metabolism and ontogeny. J Exp Med 215:1135–1152. https://doi.org/10.1084/jem.20172020.
37. Askenase MH, Han SJ, Byrd AL, Morais da Fonseca D, Bouladoux N, Wilhelm C, Konkel JE, Hand TW, Lacerda-Queiroz N, Su XZ, Trinchieri G, Grainger JR, Belkaid Y. 2015. Bone-marrow-resident NK cells prime monocytes for regulatory function during infection. Immunity 42:1130–1142. https://doi.org/10.1016/j.immuni.2015.05.011.
38. Soza A, Everhart JE, Ghany MG, Doo E, Heller T, Promrat K, Park Y, Liang TJ, Hoofnagle JH. 2002. Neutropenia during combination therapy of interferon alfa and ribavirin for chronic hepatitis C. Hepatology 36:1273–1279. https://doi.org/10.1053/jhep.2002.36502.